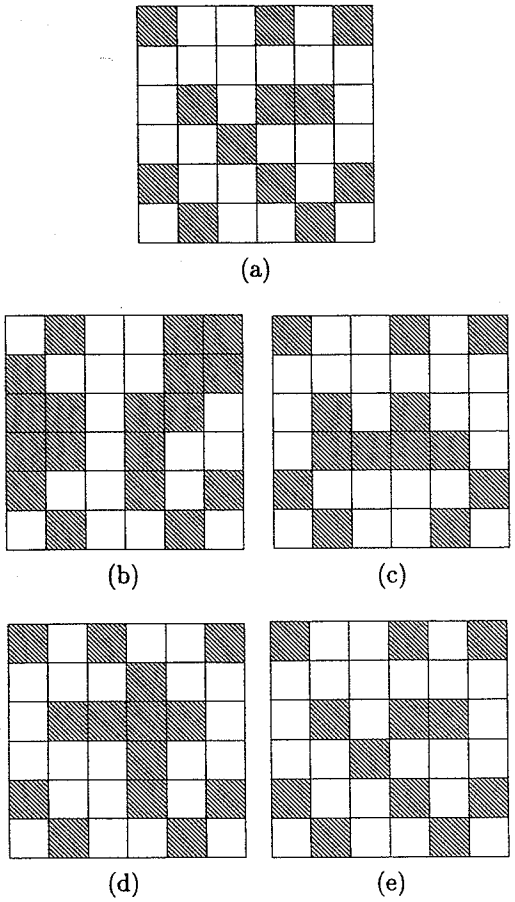

Figure 8 Reconstruction of a 2-D configuration of small cylinders. (a) True objects. (b) Best chromosome of the first generation. Fitness = 0.9963340. (c) Best chromosome of the 500th generation. Fitness = 0.9999881. (d) Best chromosome of the 1000th generation. Fitness = 0.9999915. (e) Best chromosome of the 1312th generation. Fitness = 1.0000000

that the converge is accelerated if we use 2-D GA operators, i.e., a 2-D crossover, etc., instead of 1-D operators.

VI. CONCLUSION

An iterative method has been proposed to estimate the width and location of strips. The method is based on a binary LSF combined with a GA. The numerical examples show the effectiveness of the proposed method.

Although the binary LSF–GA method proposed here is applicable to two-dimensional metallic objects of arbitrary cross section, in order to accelerate the convergence rate, it is desirable to improve the GA used here to be suitable for the 2-D objects. This is a topic for future study.

REFERENCES

1. A. Roger, "Newton-Kantorovitch Algorithm Applied to an Electromagnetic Inverse Problem," *IEEE Trans. Antennas Propagat.*, Vol. AP-29, Mar. 1981, pp. 232–238.
2. D. Colton, "The Inverse Electromagnetic Scattering Problem for a Perfectly Conducting Cylinder," *IEEE Trans. Antennas Propagat.*, Vol. AP-29, Mar. 1981, pp. 364–368.
3. C.-C. Chiu and Y.-W. Kiang, "Microwave Imaging of Multiple Conducting Cylinders," *IEEE Trans. Antennas Propagat.*, Vol. 40, Aug. 1992, pp. 933–941.
4. R. E. Kleinman and P. M. van den Berg, "Two-Dimensional Location and Shape Reconstruction," *Radio Sci.*, Vol. 29, July–Aug. 1994, pp. 1157–1169.
5. W. C. Chew and G. P. Otto, "Microwave Imaging of Multiple Conducting Cylinders Using Local Shape Functions," *IEEE Microwave Guided Wave Lett.*, Vol. 2, July 1992, pp. 284–286.
6. G. P. Otto and W. C. Chew, "Microwave Inverse Scattering—Local Shape Function Imaging for Improved Resolution of Strong Scatterers," *IEEE Trans. Microwave Theory Tech.*, Vol. 42, Jan. 1993, pp. 137–141.
7. W. H. Weedon and W. C. Chew, "Time-Domain Inverse Scattering Using the Local Shape Function (LSF) Method," *Inv. Prob.*, Vol. 9, Oct. 1993, pp. 551–564.
8. C.-C. Chiu and P.-T. Liu, "Image Reconstruction of a Perfectly Conducting Cylinder by the Genetic Algorithm," *Proc. Inst. Elect. Eng., Microwaves, Antennas Propagat.*, Vol. 143, June 1996, pp. 249–253.
9. D. E. Goldberg, *Genetic Algorithms in Search, Optimization an Machine Learning*, Addison-Wesley, Reading, MA, 1989, Chap. 1–4.
10. R. L. Haupt, "An Introduction to Genetic Algorithms for Electromagnetics," *IEEE Antennas Propagat. Mag.*, Vol. 37, Apr. 1995, pp. 7–15.
11. D. S. Weile and E. Michielssen, "Genetic Algorithm Optimization Applied to Electromagnetics: A Review," *IEEE Trans. Antennas Propagat.*, Vol. 45, Mar. 1997, pp. 343–353.
12. W. C. Chew, *Waves and Fields in Inhomogeneous Media*, Van Nostrand Reinhold, New York, 1990, App. D.

CCC 0895-2477/97

VALIDATION OF THE FINITE-DIFFERENCE TIME-DOMAIN METHOD FOR NEAR-FIELD BIOELECTROMAGNETIC SIMULATIONS

Cynthia M. Furse,[1] Quishan Yu,[1] and Om P. Gandhi[1]
[1] Department of Electrical Engineering
University of Utah
Salt Lake City, Utah 84112

Received 8 July 1997

ABSTRACT: *Validations of the accuracy of the FDTD method for near-field simulations are critical at this time to assess the accuracy of the FDTD method for the simulation of personal communication devices. Excellent comparisons between the FDTD method and analytical or measured results are shown for a dipole antenna next to a layered half-space, a layered box, and a sphere, and also an infinitesimal dipole near a sphere. © 1997 John Wiley & Sons, Inc.* Microwave Opt Technol Lett 16: 341–345, 1997.

Key words: *finite-difference time-domain method; bioelectromagnetic simulations; near-field simulations*

I. INTRODUCTION

The finite-difference time-domain (FDTD) method has become a popular numerical tool for analyzing the coupling of wireless communication devices to the human head [1]. This application requires modeling antenna configurations in the

very near field of the head. Although the FDTD method has been extensively validated against analytical and measured results for sources in the far field coupled to a variety of geometries including square and cylinders [2], spheres [3], plates [4], layered half-spaces [5], and complicated geometries such as airplanes [6], such rigorous validations have not previously been done for near-field sources.

Assessment of the accuracy of the FDTD method for near-field simulations is particularly important at this time, as it is considered an acceptable method to assess the compliance of wireless devices with newly mandated FCC guidelines [7]. In particular, in the near-field region where fields are varying as $1/r^3$, there could be some question if the FDTD method can correctly predict these rapidly varying fields. This paper demonstrates the accuracy of the method by comparing simulated results with measured, analytical, or MMP results for near fields or specific absorption rates (SARs) for a dipole antenna next to a layered half-space, a layered cube, and a sphere, and also for an infinitesimal dipole next to a sphere. The excellent agreement obtained gives confidence that the FDTD method can provide accurate results for near-field simulations. This range of test cases also provides a set of canonical test cases which can be used to validate FDTD codes or other numerical codes for near-field applications.

II. PLANAR GEOMETRIES

A. Dipole Antennas near a Two-Layered Half-Space. The first validation is for a dipole antenna very near a layered half-space. An exact, analytical solution, based on expansion of the fields from the dipole and enforcement of the boundary conditions at the planar surfaces, is given in [8] for a 900 MHz dipole of length $l = 12$ cm located at a distance $d_o = 2$ cm away from the half-space. The first layer is 1 cm thick with $\varepsilon_r = 5.977$ and $\sigma = 0.00913$ S/m (approximately the properties of skull), and the second layer is infinitely thick with $\varepsilon_r = 50.2852$ and $\sigma = 1.3423$ S/m (approximately the properties of brain).

For the FDTD model, a cell size of 5 mm is used in the horizontal (x, y) directions, and 9.23 mm in the vertical (z) direction. The second layer is supposed to be infinitely thick, which is modeled by a thickness of 24.5 cm, sufficiently thick to attenuate all of the fields to well below 1% of their peak values before the end of the material is reached. In the x- and z-directions, where the space is also theoretically infinite, the box is taken to be 12 cm in the x-direction and 33.3 cm in the z-direction. Some edge effects were observed at the edges of this box, but these effects did not alter the results at the central axis, which are of interest in this case. The simulation was run for ten cycles, but convergence of the SAR values was observed after about eight cycles.

Figure 1 shows the magnitude of the electric field along the central y-axis, comparing the analytical solution [8, Table 1] with the values calculated by the FDTD method. Values are normalized to a feedpoint current of 100 mA rms.

The close agreement of the FDTD solutions to the analytical and MMP solutions for a dipole antenna in front of an infinite layered half-space gives good confidence in the FDTD's ability to correctly model antennas in close proximity to the absorbing material. The following simulation analyzes the effect of a finite-sized model on the FDTD solution.

B. Dipole Antenna near an Absorbing Box. The second validation is for a dipole antenna near an absorbing box. This is similar to the first validation, except that the box is finite, and comparison is made to the data measured in our laboratory.

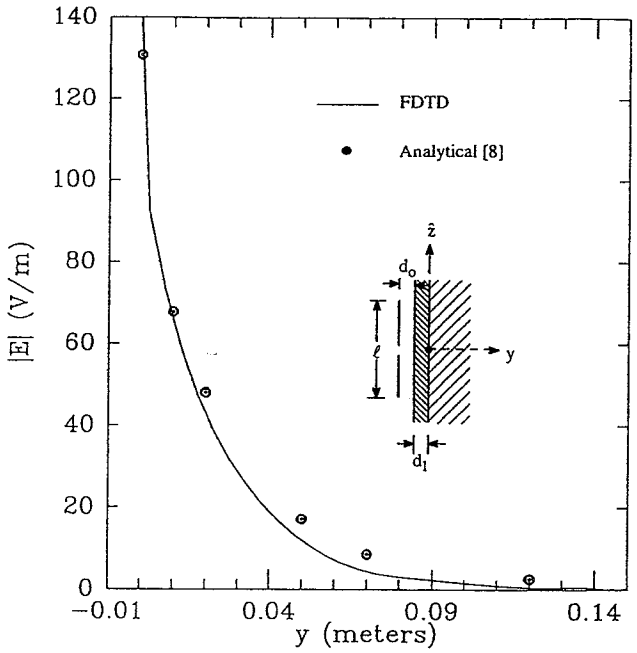

Figure 1 Magnitude of the electric field along the y-axis for a dipole in front of a layered half-space. Values are compared for the FDTD simulation and analytical results [8]

The 174 mm long dipole operating at 840 MHz is located a distance d_o in the y-direction from the box, with the feedpoint centered in front of the box. The box is $28 \times 15.5 \times 49$ cm^3 in the x, y, z-directions, respectively.

The box is made of 6.35 mm thick acrylic glass (assumed to be polystyrene with $\varepsilon_r = 2.55$). Since the cell sizes used in this simulation are slightly larger than the thickness of the acrylic, the effective dielectric constant for the glass is calculated from the formula [1]

$$\varepsilon_{\text{eff}} = \frac{\varepsilon_r \Delta}{\varepsilon_r(\Delta - w) + w} \tag{1}$$

where Δ is the size of the FDTD cell (or, in this case, two cells), w is the thickness of the acrylic, and ε_r is the dielectric constant of polystyrene. This formula is derived by finding the average fields at the air–acrylic interface and setting them equal to the fields in a larger sized cell, giving the smaller effective dielectric constant given in (1). The box is filled with brain-simulating material with $\varepsilon_r = 41.1$ and $\sigma = 1.22$ S/m.

Figure 2 shows the SAR distributions along the y-axis, and Figure 3 shows the SAR distributions along the z-direction (perpendicular to the dipole and 7 mm from the inside edge of the acrylic box), comparing the FDTD simulations and measurements for various distances d_o between the dipole and the box. The FDTD simulation use a cell size of $\Delta z = 3.053$ mm and $\Delta x = \Delta y = 2.917$, 2.8125, 3.056, and 3 mm for the separation distances between the antenna and the box of $d_o = 17.5$, 22.5, 27.5, and 33 mm, respectively. The vertical cell size Δz was chosen to precisely model the height of the dipole, and the horizontal cell sizes Δx and Δy were chosen to precisely model the separation distance d_o. Values which are used for ε_{eff} of the surface layer of thickness 6.35 mm are 2.95, 3.19, 2.71, and 2.80 for the four different cell sizes,

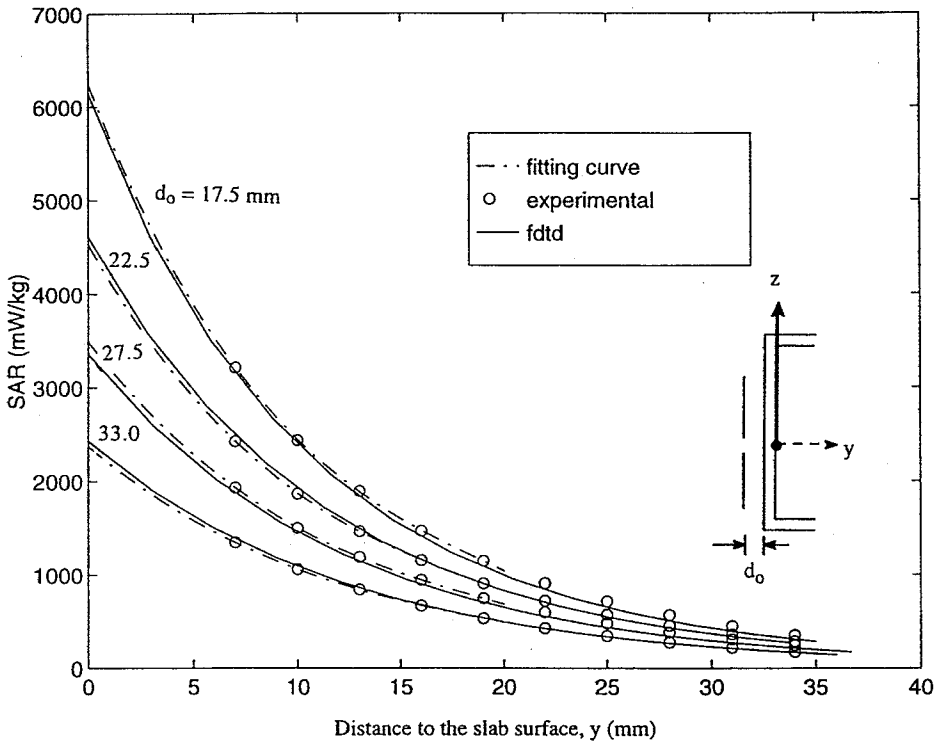

Figure 2 SAR distribution along the y-axis for a half-wave dipole antenna in front of a box filled with brain-simulant material. Values are given for different separation distances d_o between the dipole and box, and are compared with measured data

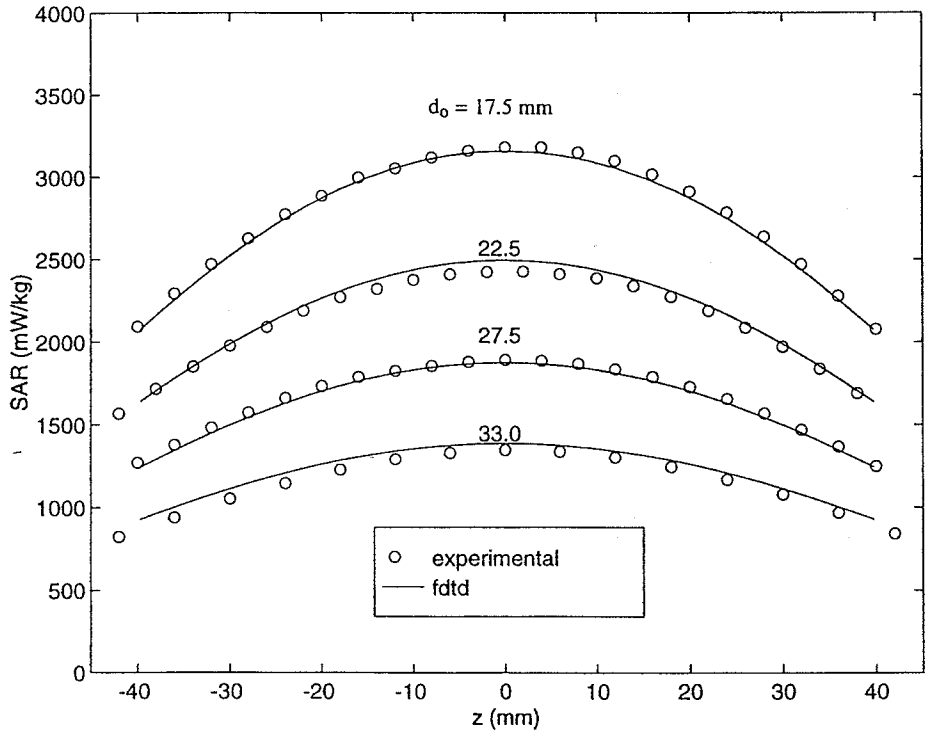

Figure 3 SAR distribution along the z-axis (parallel to the antenna) 7 mm inside the brain-simulant material for the same test case as Figure 2. Values are given for different separation distances d_o between the dipole and box, and are compared with measured data

respectively. Simulations were run for 2500 time steps, and convergence was observed after about 5000 time steps, and convergence was observed after about 3000 time steps. Values were normalized to a total radiated power of 500 mW.

Measurements of the SARs were taken using a Narda Model 8021 B E-field probe inserted along the y-axis.

Excellent agreement between measured and simulated values in Figures 2 and 3 is interesting in several respects. First, it demonstrates the accuracy of both the measurements and simulations in this very near-field region. Second, since the physical dimensions of the probe make it impossible to measure closer than 7 mm to the front of the box, a third-order spline polynomial was fit to the measured data, and is shown as a dashed line in Figure 2. This would be necessary to accurately measure the 1 g averaged SAR values for any realistic simulation since the peak fields, and hence the peak SARs, occur at the very front of the object, nearest the antenna. The excellent agreement between the simulated data and the measured data extrapolated to the front of the box is not surprising, as the fields are known to decay as $1/r^3$ in this region, and a third-order fit should provide accurate data.

III. SPHERICAL GEOMETRY VALIDATIONS

The test case simulations in Section III give good confidence in the FDTD method's ability to correctly predict the fields and SAR distribution within planar phantoms as a function of distance between the antenna and the phantom. These simulations do not require modeling of curved surfaces, which are associated with the high-resolution head models required for the analysis of many wireless communication devices. FDTD has been demonstrated to accurately model absorbing spheres for far-field plane-wave exposures [3], and the test cases in this section demonstrate FDTD's ability to correctly analyze fields or SARs within spherical absorbers for near-field sources. For this FDTD analysis, the curved object was modeled using "staircasing," or cubical cells filling the curved object.

A. Infinitesimal Dipole near a Sphere. For this test case, an infinitesimal Hertzian dipole is located 1.5 cm away from a 20 cm diameter brain-equivalent sphere [9]. The frequency is 900 MHz, and the properties taken for the sphere are $\varepsilon_r = 43$ and $\sigma = 0.83$ S/m. The infinitesimal dipole is modeled as a single Ez feedpoint location, without the surrounding wire antenna used in previous test cases. The FDTD cell size is $\Delta x = \Delta y = \Delta z = 5$ mm, which makes the sphere 40 cells in diameter. Care was taken modeling the sphere, so that the front edge contained five cells, rather than just one, which was critical to obtain FDTD agreement with analytical results.

Figure 4 shows the relative SAR along the y-axis from the front edge of the sphere calculated using the FDTD method and compared to an analytical solution based on the Bessel function expansion [9].

B. Dipole Antenna Near a Sphere. An approximately half-wave dipole antenna ($l = 17.3$ cm) is modeled 2.5 cm from a 20 cm diameter brain-equivalent sphere ($\varepsilon_r = 55$, $\sigma = 1.4$ S/m) at 840 MHz. This is modeled with an FDTD cell size of $\Delta x = \Delta y = 5$ mm and $\Delta z = 5.9655$ mm, and the simulation was run for 1500 time steps.

Figure 5 shows the SAR distribution along the y-axis from the front edge of the sphere comparing the FDTD and MMP

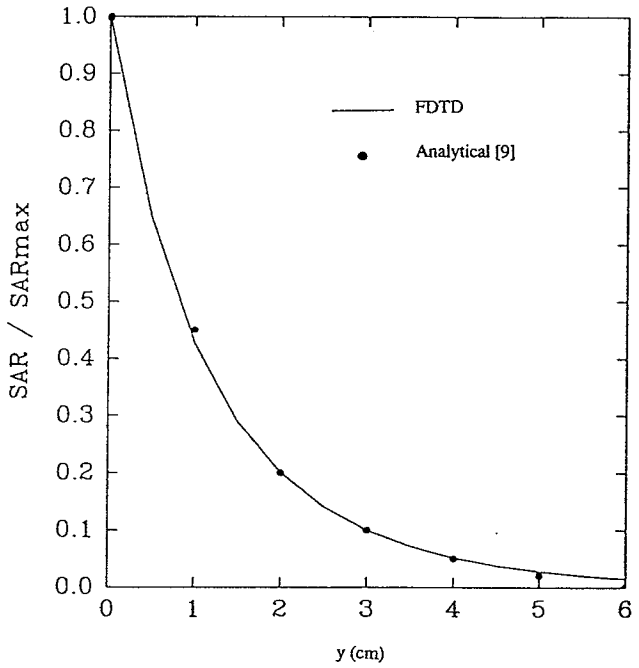

Figure 4 Relative SAR distribution along the y-axis for an infinitesimal dipole in front of a homogeneous brain-equivalent sphere. Values are compared with analytical results [9]

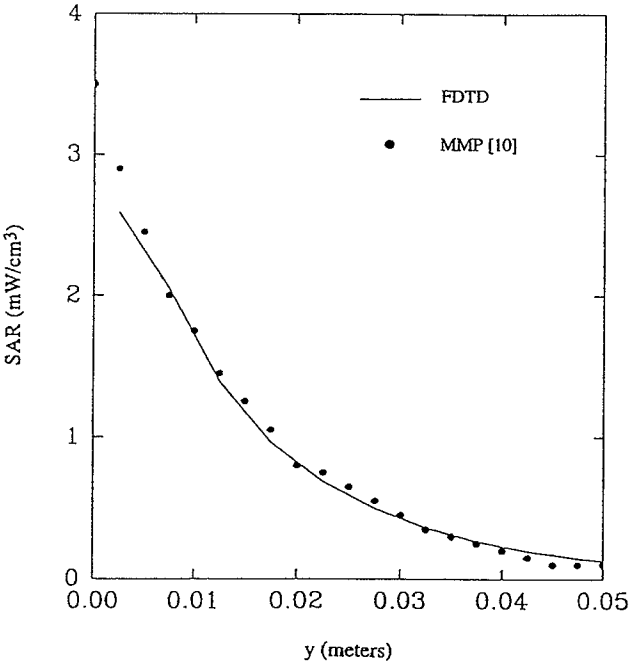

Figure 5 SAR distribution along the y-axis of a homogeneous brain-equivalent sphere excited by a half-wave dipole antenna. Values are compared with the MMP solution of [10]

[10] simulation results. The excellent agreement between FDTD and analytical or MMP results observed in these two simulations gives confidence that the FDTD method can accurately model curved absorbing objects for near-field simulations.

IV. CONCLUSIONS

The FDTD method has been demonstrated to give excellent comparisons with analytical, measured, and MMP results for the fields or SARs within planar and spherical absorbing tissue phantoms very near dipole antenna sources for parameters approximately representing cellular telephone simulations. The excellent agreement obtained validates the FDTD method for near-field simulations. Additional work is ongoing in our laboratory to assess the accuracy of the FDTD method for more complicated sources such as realistic cellular telephones [11, 12] by comparing calculated near-field SARs and far-field radiation patterns with measurements.

REFERENCES

1. O. P. Gandhi, G. Lazzi, and C. M. Furse, "Electromagnetic Absorption in the Human Head and Neck for Mobile Telephones at 835 and 1900 MHz," *IEEE Trans. Microwave Theory Tech.*, Vol. 44, 1996, pp. 1884–1897.
2. K. Umashankar and A. Taflove, "A Novel Method to Analyze Electromagnetic Scattering of Complex Objects," *IEEE Trans. Electromag. Compat.*, Nov. 1982, pp. 397–124.
3. R. Holland, L. Simpson, and K. S. Kunz, "Finite-Difference Analysis of EMP Coupling to Lossy Dielectric Structures," *IEEE Trans. Electromag. Compat.*, 1980, pp. 203–209.
4. A. Taflove, K. R. Umashankar, and T. G. Jurgens, "Validation of FD-TD Modeling of the Radar Cross Section of Three-Dimensional Structures Spanning up to Nine Wvelengths," *IEEE Trans. Antennas Propagat.*, 1985, pp. 662–666.
5. M. L. Oristaglio and G. W. Hohmann, "Diffusion of Electromagnetic Fields into a Two-Dimensional Earth: A Finite-Difference Approach," *Geophys.*, 1984, pp. 870–894.
6. K. S. Kunz and K.-M. Lee, "A Three-Dimensional Finite-Difference Solution of the External Response of an Aircraft to a Complex Transient EM Environment: Part II—Comparison of Predictions and Measurements," *IEEE Trans. Electromagn. Compat.*, 1978, pp. 333–341.
7. FCC 96-326, "Guidelines for Evaluating the Environmental Effects of Radiofrequency Radiation," Aug. 1, 1996, available from Federal Communications Commission, Washington, DC 20554.
8. R. W. P. King, "The Electromagnetic Field of a Horizontal Electric Dipole in the Presence of a Three-Layered Region: Supplement," *J. Appl. Phys.*, Vol. 74, 1993, pp. 4845–4848.
9. G. Dhondt and L. Martens, "A Canonical Case with an Analytical Solution for the Comparison of Electromagnetic Field Solvers," *Proc. COST 244 Meeting on Reference Models for Bioelectromagnetic Test of Mobile Communication Systems*, D. Suminic, Ed.
10. N. Kuster and Q. Balzano, "Energy Absorption Mechanism by Biological Bodies in the Near Field of Dipole Antennas about 300 MHz," *IEEE Trans. Veh. Technol.*, Vol. 41, 1992, pp. 17–23.
11. G. Lazzi and O. P. Gandhi, "On Modeling and Personal Dosimetry of Cellular Telephone Helical Antennas with the FDTD Code," submitted to *IEEE Trans. Antennas Propagat.*
12. G. Lazzi, S. S. Pattnaik, C. M. Furse, and O. P. Gandhi, "Comparison of FDTD-Computed and Measured Radiation Patterns of Commercial Mobile Telephones in Presence of the Human Head," submitted to *IEEE Trans. Antennas Propagat.*

CCC 0895-2477/97

THIRD-ORDER SATURATION EFFECTS IN A HELIX TRAVELING-WAVE TUBE UNDER EULERIAN APPROXIMATIONS

S. K. Datta,[1] P. K. Jain,[2] and B. N. Basu[2]
[1] Microwave Tube Research and Development Center
Defence Research and Development Organisation
Bel Complex, Bangalore 560013, India
[2] Centre of Research in Microwave Tubes
Department of Electronics Engineering
Institute of Technology
Banaras Hindu University
Varanasi 221005, India

Received 21 July 1997

ABSTRACT: *A third-order nonlinear equation for the circuit electric field was formulated for a helix traveling-wave tube under Eulerian fluid-dynamical approximations. The equation was solved by the method of successive approximations and interpreted for circuit power. When the third-order effects were included in the analysis, the saturation behavior of the device, with respect to both interaction length and RF input power, was found to be similar in nature to that predicted by Lagrangian analysis, agreeing well under backed-off conditions. The values of RF input power and interaction length corresponding to saturation found by the present Eulerian method were greater than those found by Lagrangian method. Although the present Eulerian technique has an inherent limitation of accuracy as compared to the Lagrangian one, it does not involve large-scale numerical integration, gives a closed-form solution, and hence becomes less encumbered. © 1997 John Wiley & Sons, Inc.* Microwave Opt Technol Lett 16: 345–349, 1997.

Key words: *microwave tubes; traveling-wave tubes; nonlinear Eulerian analysis*

1. INTRODUCTION

Wideband helix traveling-wave tubes (TWTs) continue to be important in microwave communication systems. The device enjoys unparalleled bandwidth, and the present-day technological innovations have considerably enhanced the other performance characteristics of the device such as power, operating frequency, efficiency, life, and reliability. The performance of the device is, however, likely to be degraded by the nonlinearity of the electron beam which is used as one of the constituents of the device [1]. The nonlinearity causes effects such as harmonic generation, intermodulation distortion, saturation effects, etc., in the device. Paschke, in a series of papers [2–4], analyzed a modulated electron beam for its nonlinear behavior by Eulerian dynamics. The method of analysis, he claims, would dispel the widespread belief that, because of electron overtaking, Eulerian model must break down at large power levels [3]. He demonstrated that, at least for a beam plasma frequency much less than the signal frequency, the model would give an adequate prediction of the behavior of the beam up to the saturation level. Paschke, however, did not consider in his analysis the interaction of the electron beam with any other medium like another beam, as in a double-stream amplifier (DSA), or a plasma as in a beam–plasma amplifier (BPA) [5–7]; nor did he consider such interaction with a surrounding circuit, as in a TWT [8]. Paschke's Eulerian nonlinear analysis was extended up to the second order, and was found to be good enough for the prediction of behavior like second harmonic, sum- and difference-frequency generation in a DSA and a BPA [5, 6]. The nonlinearity was also reported to be extended up to the third order to study saturation effects in a BPA [7]. The